

# Chapter 1

## Inherent Optical Property Measurement Concepts: Physical Principles and Instruments

Scott Pegau<sup>1</sup>, J. Ronald V. Zaneveld<sup>1</sup> and James L. Mueller<sup>2</sup>

<sup>1</sup>*College of Oceanographic and Atmospheric Sciences, Oregon State University, Corvallis*

<sup>2</sup>*Center for Hydro-Optics and Remote Sensing, San Diego State University, California*

### 1.1 INTRODUCTION

The Inherent Optical Properties (IOP) of a medium, which describe absorption and scattering interactions that modify a vector light field propagating through it, are defined in Vol. I, Ch. 2, Sect. 2.4 of this protocol document. Geometric conventions and notation underlying definitions of, and relationships between IOP and radiative transfer in the medium are described in Section 2.2 of Vol. I, Ch. 2. The roles of the IOP in radiative transfer descriptions and models of light propagation in the sea are also introduced in Vol. I, Ch. 2, and appear elsewhere in many of the Volumes and Chapters of this protocol document.

The chapters of this volume (Vol. IV) describe the conceptual background, instrument characteristics, and methods of calibration, field measurements and data analysis for determining the IOP of seawater. The scope of this protocol volume is limited to practical methods for using commercially available instruments<sup>1</sup> to determine the IOP identified in Vol. I, Chapter 3 (Table 3.1) of *Ocean Optics Protocols for Satellite Ocean Color Sensor Validation, Rev. 4*. The scope of the present volume does not include applications of measured IOP to aspects of ocean color sensor validation that are described elsewhere in the document. The role of IOP in the determination of *Exact Normalized Water-Leaving Radiance*  $L_{\text{WN}}^{\text{ex}}(\lambda)$  as a function of wavelength  $\lambda$ , for example, is discussed in Vol. III, Chapter 4.

In this chapter we extend the IOP definitions and relationships of Vol. I, Ch. 2 to develop the theoretical and mathematical bases for practical instrument concepts and methods for measuring IOP in seawater. Instruments will be described to measure, *in situ* at depth  $z$ , the beam attenuation coefficient  $c(z, \lambda)$ , the volume absorption coefficient  $a(z, \lambda)$ , and the volume scattering function (VSF)  $\beta(z, \lambda, \psi)$  at one or more scattering angles  $\psi$ . Spectrophotometric laboratory methods are also described in detail for determining absorption coefficients from filtered, discrete water samples. Methods of data analysis are described to determine, from combinations of these measurements, the volume scattering coefficient  $b(z, \lambda)$  and backscattering coefficient  $b_b(z, \lambda)$ .

We do not consider instrument concepts or methods for measuring either fluorescence, or Raman scattering, in Vol. IV. Even though the Raman and fluorescence cross-sections of water, suspended particles and dissolved materials are also IOP of seawater, **only elastic scattering processes** are considered in this volume.

In the remainder of Vol. IV, we will ordinarily omit the explicit notation identifying IOP variables as functions of depth  $z$  in the water column. This is partly a desire for simplifying the notation, but the more important motive is to avoid confusing global coordinates (geographic location and vertical depth in the water column) with local coordinates (optical axes and normal planes) used to describe photon-matter interactions and measurement concepts.

---

<sup>1</sup> Certain commercial equipment, instruments, or materials are identified in this chapter to foster understanding. Such identification does not imply recommendation, or endorsement, by the National Aeronautics and Space Administration, nor does it imply that the materials or equipment identified are necessarily the best available for the purpose.

## 1.2 ABSORPTION AND SCATTERING PROPERTIES OF WATER, PARTICLES AND DISSOLVED SUBSTANCES

Because the IOP are additive (Vol. I, Ch. 2, Sect. 2.4), the absorption and scattering properties of natural water consists of the sums of these IOP of pure water, suspended particles, dissolved substances and turbulence. It is very difficult to experimentally determine the absorption of pure water in the laboratory, due principally to the difficulty of making and maintaining pure water during the course of an experiment. Nevertheless, there have been several successful experiments (several are cited below), over the past few decades, and the spectral absorption and scattering coefficients of pure water are reasonably well known. Using this information, several types of IOP instruments are calibrated by measuring their responses using pure water as an “optical standard”. Thus, the calibrated responses of these instruments in field measurements represent the IOP of particles and dissolved material, independent of water. IOP.

From another perspective, the general characteristics of absorption and scattering properties vary spectrally, and in the case of scattering angularly, between the different optically important constituents of seawater. The contrast in angular distribution characteristics of scattering by water and by particles can be an important element of instrument design concepts.

### *Absorption by Pure Water*

The spectral values recommended in Vol. I, Ch. 2 (Sect. 2.4) for the volume absorption coefficients of pure water,  $a_w(\lambda) \text{ m}^{-1}$ , are those of Sogandares and Fry (1997) for wavelengths between 340 nm and 380 nm, Pope and Fry (1997) for wavelengths between 380 nm and 700 nm, and Smith and Baker (1981) for wavelengths between 700 nm and 800 nm. Here, for wavelengths  $> 700$  nm we recommend values calculated by Van Zee *et al.* (2002) from the imaginary part of the refractive indices for pure water measured by Kou *et al.* (1993). The composite  $a_w(\lambda)$  spectrum derived from these sources is listed in Table 1.1, together with the linear temperature dependency  $\frac{\partial a_w(\lambda)}{\partial T} [\text{m}^{-1}\text{°C}]$  reported by Pegau and Zaneveld (1993) and Pegau *et al.* (1997).

### *Absorption by Suspended Particulates and Colored Dissolved Organic Material (CDOM)*

Variations in the spectral absorption of natural waters result directly from variations in the concentrations and chemical compositions of material substances distributed within the water volume. These absorbing materials may be present in seawater either in suspended particulates, such as pigment-bearing phytoplankton, or as solutes (*i.e.* CDOM). Fig. 1.1a illustrates qualitative comparisons between the absorption spectrum of pure water,  $a_w(\lambda)$  (Table 1.1), a non-dimensional *Chl*-specific absorption spectrum of phytoplankton pigment concentration,  $a_{chl}^*(\lambda)$  (Prieur and Sathyendranath 1981), and a typically exponential absorption spectrum of CDOM  $a_g(\lambda)$  (Bricaud *et al.* 1981). The amplitude of each absorption spectrum in Fig. 1.1a is arbitrarily scaled to illustrate the characteristic difference in shapes between the constant water background absorption and two varying absorption components associated with *Chl* and CDOM concentrations. The unique shape and magnitude of the specific absorption spectrum for each individual constituent allows measured values of, *e.g.*, *Chl* and CDOM concentrations to be determined from measurements of  $a(\lambda)$  at several appropriate wavelengths. The strong inverse dependence of remote sensing reflectance on  $a(\lambda)$  (Vol. III, Ch. 4), together with the distinctive shape and magnitude characteristics of the constituents, similarly provides the physical basis for ocean color algorithms for determining their concentrations from satellite measurements of water leaving radiance at several wavelengths.

In Case 1 waters, it is often useful to assume (Gordon and Morel 1983; Morel and Maritorena 2001; Mobley and Sundman 2000) that particle absorption  $a_p(\lambda)$  is dominated by phytoplankton pigments and may be expressed as a function of *Chl* concentration [ $\text{mg m}^{-3}$ ] and a *Chl*-specific absorption spectrum  $a_{chl}^*(\lambda)$  (Prieur and Sathyendranath 1981), and that CDOM concentration is correlated with *Chl* so that  $a_g(\lambda)$  may also be calculated as

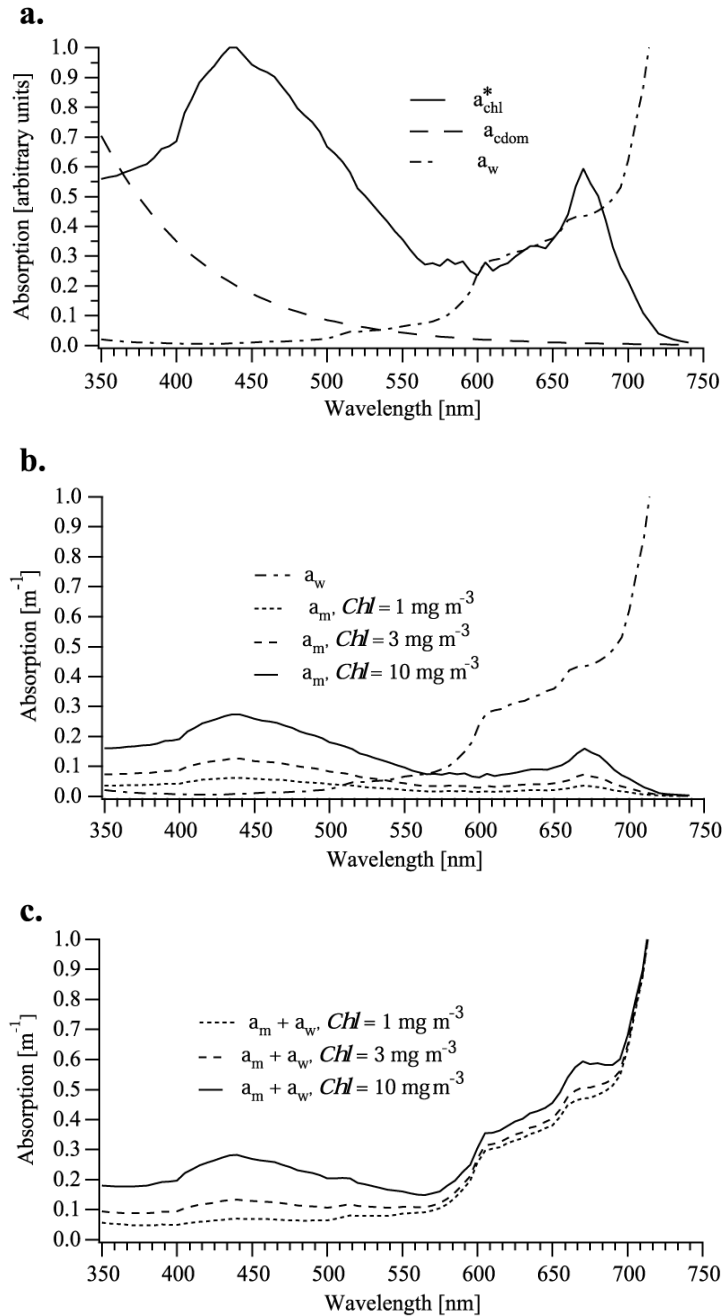


Fig. 1.1: Spectral variations of absorption in seawater. **a:** Qualitative comparison of the shapes of absorption spectra of pure water (Table 1.1), specific absorption by *Chl* (Prieur and Sathyendranath 1981), and CDOM as implemented in the HYDROLIGHT radiative transfer model (Mobley and Sundman 2000) described further by Morel and Maritorena (2001). **b:** Comparisons between  $a_w(\lambda)$ , the absorption spectrum of pure water, and  $a_m(\lambda, Chl)$ , the sum of absorption by suspended particles and CDOM for *Chl* concentrations of 1, 3 and  $10 \text{ mg m}^{-3}$ , following Mobley and Sundman (2000). An absorption meter calibrated relative to pure water would measure  $a_m(\lambda; Chl)$ . **c:** The sums of pure water and “measured” absorption spectra from panel b.



**Table 1.1:** Volume absorption and scattering coefficients for pure water,  $a_w(\lambda)$  and  $b_w(\lambda)$ , respectively. Values for  $a_w(\lambda)$  are those of Sogandares and Fry (1997) [340 to 390 nm], Pope and Fry (1997) [400 to 700 nm], and Van Zee *et al.* (2002) as derived from Kou *et al.* (1993) [705 to 750 nm]. Alternative values of  $b_w(\lambda)$  compared here are denoted (B) (Buitveld, *et al.* 1994) and (M) (Morel 1974). The linear temperature dependence of pure water absorption,  $\frac{\partial a_w(\lambda)}{\partial T}$ , is due to Pegau and Zaneveld (1993) and Pegau *et al.* (1997).

$\lambda$	$a_w$	$\frac{\partial a_w(\lambda)}{\partial T}$	$b_w$	$b_w$	$\lambda$	$a_w$	$\frac{\partial a_w(\lambda)}{\partial T}$	$b_w$	$b_w$	$\lambda$	$a_w$	$\frac{\partial a_w(\lambda)}{\partial T}$	$b_w$	$b_w$
nm	$\text{m}^{-1}$	$\text{m}^{-1}\text{ }^\circ\text{C}$	$\text{m}^{-1}$ (B)	$\text{m}^{-1}$ (M)	nm	$\text{m}^{-1}$	$\text{m}^{-1}\text{ }^\circ\text{C}$	$\text{m}^{-1}$ (B)	$\text{m}^{-1}$ (M)	nm	$\text{m}^{-1}$	$\text{m}^{-1}\text{ }^\circ\text{C}$	$\text{m}^{-1}$ (B)	$\text{m}^{-1}$ (M)
340	0.0325	0.0000	0.0104	0.0118	500	0.0242	0.0001	0.0021	0.0022	630	0.3184	0.0002	0.0008	0.0009
350	0.0204	0.0000	0.0092	0.0103	505	0.0300	0.0001	0.0020		635	0.3309	0.0000	0.0008	
360	0.0156	0.0000	0.0082	0.0091	510	0.0382	0.0002	0.0019	0.0020	640	0.3382	-0.0001	0.0008	0.0008
370	0.0114	0.0000	0.0073	0.0081	515	0.0462	0.0002	0.0018		645	0.3513	0.0000	0.0007	
380	0.0100	0.0000	0.0065	0.0072	520	0.0474	0.0002	0.0018	0.0019	650	0.3594	0.0001	0.0007	0.0007
390	0.0088	0.0000	0.0059	0.0065	525	0.0485	0.0002	0.0017		655	0.3852	0.0002	0.0007	
400	0.0070	0.0000	0.0053	0.0058	530	0.0505	0.0001	0.0017	0.0017	660	0.4212	0.0002	0.0007	0.0007
405	0.0060	0.0000	0.0050		535	0.0527	0.0001	0.0016		665	0.4311	0.0002	0.0006	
410	0.0056	0.0000	0.0048	0.0052	540	0.0551	0.0001	0.0015	0.0016	670	0.4346	0.0002	0.0006	0.0007
415	0.0052	0.0000	0.0045		545	0.0594	0.0001	0.0015		675	0.4390	0.0001	0.0006	
420	0.0054	0.0000	0.0043	0.0047	550	0.0654	0.0001	0.0014	0.0015	680	0.4524	0.0000	0.0006	0.0006
425	0.0061	0.0000	0.0041		555	0.0690	0.0001	0.0014		685	0.4690	-0.0001	0.0006	
430	0.0064	0.0000	0.0039	0.0042	560	0.0715	0.0001	0.0013	0.0014	690	0.4929	-0.0002	0.0006	0.0006
435	0.0069	0.0000	0.0037		565	0.0743	0.0001	0.0013		695	0.5305	-0.0001	0.0005	
440	0.0083	0.0000	0.0036	0.0038	570	0.0804	0.0001	0.0012	0.0013	700	0.6229	0.0002	0.0005	0.0005
445	0.0095	0.0000	0.0034		575	0.0890	0.0002	0.0012		705	0.7522	0.0007	0.0005	
450	0.0110	0.0000	0.0033	0.0035	580	0.1016	0.0003	0.0011	0.0012	710	0.8655	0.0016	0.0005	0.0005
455	0.0120	0.0000	0.0031		585	0.1235	0.0005	0.0011		715	1.0492	0.0029	0.0005	
460	0.0122	0.0000	0.0030	0.0031	590	0.1487	0.0006	0.0011	0.0011	720	1.2690	0.0045	0.0005	0.0005
465	0.0125	0.0000	0.0028		595	0.1818	0.0008	0.0010		725	1.5253	0.0065	0.0004	
470	0.0130	0.0000	0.0027	0.0029	600	0.2417	0.0010	0.0010	0.0011	730	1.9624	0.0087	0.0004	0.0005
475	0.0143	0.0000	0.0026		605	0.2795	0.0011	0.0010		735	2.5304	0.0108	0.0004	
480	0.0157	0.0000	0.0025	0.0026	610	0.2876	0.0011	0.0009	0.0010	740	2.7680	0.0122	0.0004	0.0004
485	0.0168	0.0000	0.0024		615	0.2916	0.0010	0.0009		745	2.8338	0.0119	0.0004	
490	0.0185	0.0000	0.0023	0.0024	620	0.3047	0.0008	0.0009	0.0009	750	2.8484	0.0106	0.0004	0.0004
495	0.0213	0.0001	0.0022		625	0.3135	0.0005	0.0008						

an exponential function of wavelength (Bricaud *et al.* 1981) scaled as a function of *Chl*. Fig. 1.1b shows the sum  $a_m(\lambda; Chl) = a_p(\lambda; Chl) + a_g(\lambda; Chl)$  calculated, for  $Chl = 1, 3$  and  $10 \text{ mg m}^{-3}$ , using this simple model, as implemented in one of the standard IOP specification options within the HYDROLIGHT radiative transfer model (Mobley and Sundman 2000). The subscript “m” indicates that the spectra shown in Fig. 1.1b are those that would be measured by an instrument that was calibrated using pure water as a standard reference medium (Chapter 3). The absorption of pure water  $a_w(\lambda)$  is compared with  $a_m(\lambda; Chl)$  in Fig. 1.1b, and the corresponding total absorption coefficient spectra  $a(\lambda; Chl) = a_w(\lambda) + a_m(\lambda; Chl)$  are illustrated in Fig. 1.1c. The illustrated examples are admittedly an oversimplification, but they are adequate as a basis for considering the nature of IOP components of the signal measured by an absorption meter, or transmissometer, at individual wavelengths.

### Scattering by Pure Water

The spectral values of the pure water volume scattering coefficient  $b_w(\lambda)$  recommended in Vol. I, Chapter 2 (Sect. 2.4) are those of Morel (1974), as reported by Smith and Baker (1981). Following Van Zee *et al.* (2002), however, we recommend here that preference be given to the  $b_w(\lambda)$  scales of Buiteveld, *et al.* (1994). Both scales are listed in Table 1.1 for comparison. The difference between the two scales is  $\leq 0.0001 \text{ m}^{-1}$  at wavelengths  $> 475 \text{ nm}$ , increases to  $\leq 0.0005 \text{ m}^{-1}$  as wavelength decreases to  $400 \text{ nm}$ , and increases further to  $\leq 0.0014 \text{ m}^{-1}$  at  $340 \text{ nm}$ . In no instance does the difference closely approach the  $0.005 \text{ m}^{-1}$  measurement uncertainty of beam attenuation and absorption meters that are commercially available to date.

The angular distribution of the molecular scattering phase function  $\beta_w^0(\psi)$ , as approximated with equation (2.29) [Vol. I, Ch. 2], is illustrated in Fig. 1.2. The magnitude of  $\beta_w^0(\psi)$  represents the probability that a photon scattering interaction with a water molecule will redirect the photon path direction by an angle  $\psi$  measured from its original path. The shape of  $\beta_w^0(\psi)$  is sometimes referred to as “isotropic” in the literature, a characterization that is true only in that the function is axially symmetric and the probabilities of forward and backward scattering are equal.

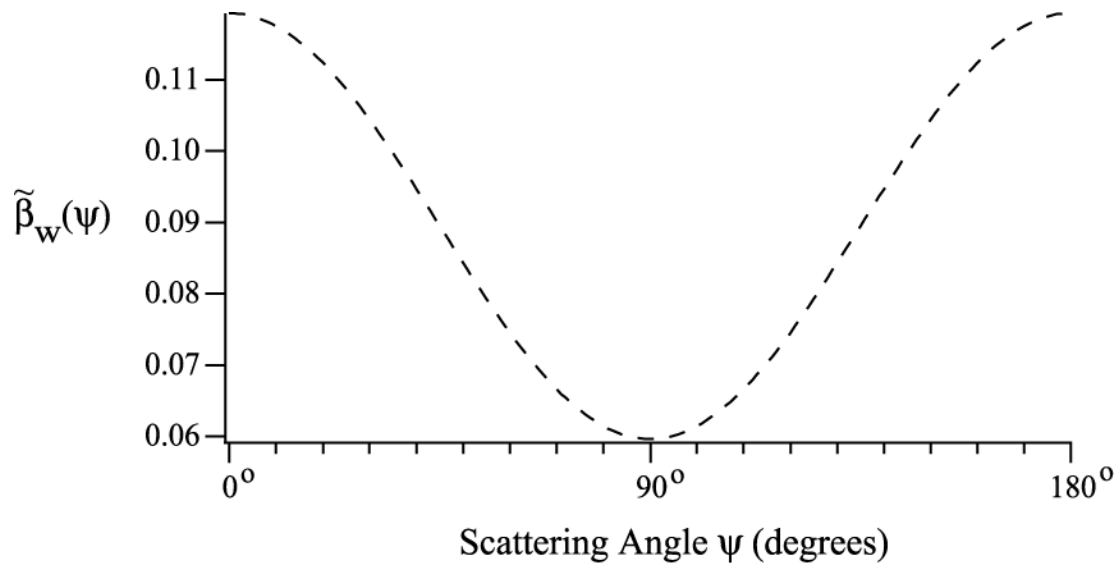


Fig. 1.2: The dashed curve represent the angular distribution of the scattering phase function for pure water, calculated using the approximate Rayleigh scattering model [equation (2.29) of Vol. I, Ch. 2].

### Scattering by Particles

In many natural waters, the volume scattering coefficient for particles  $b_p(\lambda)$  is comparable to, or larger than, that of pure water. Moreover, the shape of a particle scattering phase function  $\beta_w^o(\lambda, \psi)$ , an example of which is illustrated as the solid curve in Fig. 1.3, is strongly peaked - by several orders of magnitude - in the forward direction. The extreme contrast between the angular probability distributions of particulate and molecular scattering (the dashed curve in Fig. 1.3) are important factors that must be considered when designing transmissometers and scattering meters for use in the sea.

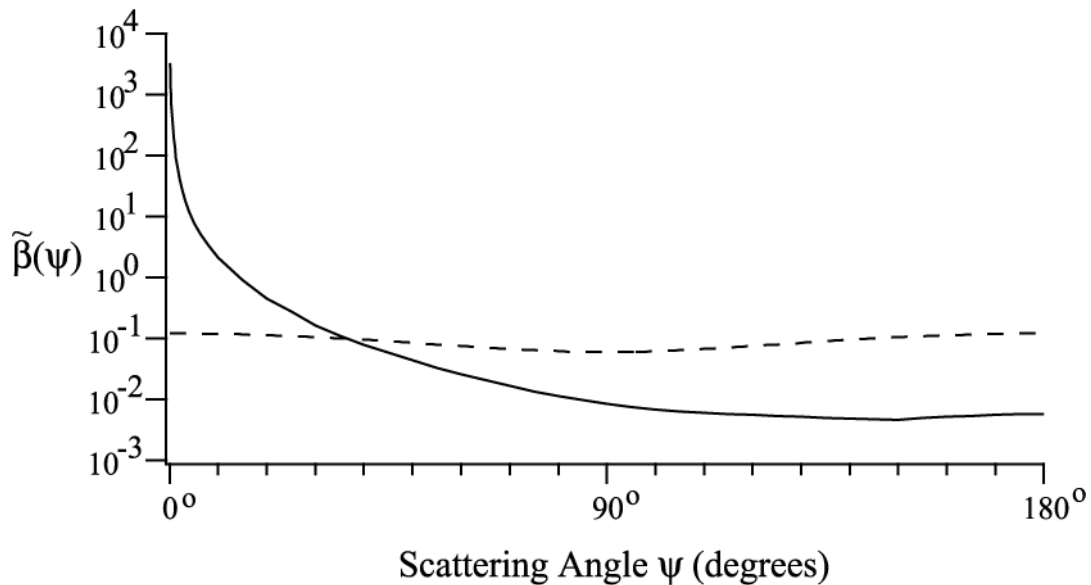


Fig. 1.3: The solid curve is an example of a measured scattering phase function for ocean water dominated by particle scattering (Petzold 1972; San Diego Harbor Stn. 2040). The dashed curve is the pure water phase function from Fig. 1.2, shown here for comparison.

### Scattering by Turbulence

Random fluctuations in water density, induced by turbulence, act to steer photons through very small angles in the forward direction, and therefore, scattering by turbulence is also strongly peaked, by orders of magnitude, in the forward direction. Because turbulent fluctuations are completely random in space and time, the variance of photons scattered by turbulence at small angles is much greater than the variance associated with small angle scattering by particles (Bogucki *et al.* 1998)

## 1.3 RADIANT FLUX TRANSMISSION MEASUREMENT CONCEPTS

### Geometry and Nomenclature

In Fig. 1.4 the origin of a local instrument coordinate system is placed at the exit aperture of a source of monochromatic radiant flux  $\Phi_o(\lambda, 0, 0, 0)$  [in  $\mu\text{W nm}^{-1}$ ]<sup>2</sup> directed as a collimated beam along the positive  $z_m$ -axis (see also Fig. 2.2 in Vol. I, Ch. 2). The subscript “m” associated with the coordinate basis vectors  $(\hat{\mathbf{x}}_m, \hat{\mathbf{y}}_m, \hat{\mathbf{z}}_m)$  in Fig. 1.4 indicate that the local “measurement” coordinate frame is associated with a particular instrument concept, as distinguished from global coordinates defining positions and directions in the extended medium (cf Figs. 2.1 and 2.2 in Vol. I, Ch. 2). The local instrument coordinate framework is related to global coordinates by a translation and rotations that are arbitrary and need not be considered in the present context<sup>3</sup>.

The direction associated with an optical path vector intersecting the transmitted beam axis ( $z_m$ -axis) is described by the angle pair  $(\psi, \varphi)$ , where  $0 \leq \psi \leq \pi$  is measured from the  $z_m$ -axis and  $0 \leq \varphi \leq 2\pi$  is measured from the  $x_m$ -axis counterclockwise in the  $x_m y_m$ -plane. The variable  $r$ , with various subscripts, will denote geometric distance along any such optical path<sup>4</sup>. Directional radiant flux at distance  $r$  from a source, or from a scattering interaction site within the transmitted beam, is denoted  $\Phi(\lambda, r, \psi, \varphi)$ . In Fig. 1.4 for example, radiometric flux scattered into direction  $(\psi, \varphi)$  at position  $\mathbf{x}_s^V$  is denoted as  $\Phi_s(\lambda, 0, \psi, \varphi)$ , and the scattered flux transmitted in that direction to Detector 2, at position  $\mathbf{x}_D^V$ , as  $\Phi_s(\lambda, r_D, \psi, \varphi)$ . Radiometric flux within the beam transmitted to a point on the  $z_m$ -axis at distance  $r$  from the source is denoted,  $\Phi_T(\lambda, r, 0, \bullet)$ , where the dot indicates that  $\varphi$  is indeterminate when  $\psi = 0$  or  $\psi = \pi$ . In particular, the flux transmitted from the source to Detector 1 is  $\Phi_T(\lambda, r_T, 0, \bullet)$ .

#### *Transmittance and Beam Attenuation*

The shaded rectangle overlaid on the extended  $z_m$ -axis in Fig. 1.4 schematically illustrates a cylinder (of cross sectional area  $\Delta s$ ) representing the collimated beam of radiant flux transmitted from the source to Detector 1. The gradient in shading represents the exponential decrease in  $\Phi_T(\lambda, r, 0, \bullet)$  with increasing distance  $r$ , as photons interact with the medium and are absorbed and scattered out of the beam. During transmission over a path interval from  $r$  to  $r + \Delta r$ , the fraction of radiant flux absorbed in the volume  $\Delta s \Delta r$  is **spectral absorptance**,  $A(\lambda)$  and the fraction of flux scattered out of the beam direction in that volume is **spectral scatterance**  $B(\lambda)$  (see Vol. I, Chapter 2, Sect. 2.4).

One could envision superimposing a lightly shaded “cloud” on Fig. 1.4 to visualize scattered photons escaping from the beam in all directions, but this would not indicate the directional nature of the scattering losses. Instead, the scattering process is schematically illustrated in Fig. 1.4 as a mottled, shaded path of photons scattered in a particular direction  $(\psi, \varphi)$  at a single location  $\mathbf{x}_s^V$  in the beam<sup>5</sup>. At this on-axis location,  $\mathbf{x}_s^V$ , similar beams could be drawn in any other direction to visually indicate scattered flux intensity and its subsequent transmittance and attenuation in the new direction. The same type of graphic could be drawn anywhere along the optical path, and if many were combined we’d generate the

<sup>2</sup> The choice of these units, rather than, *e.g.*,  $\text{W m}^{-1}$ , is customary in ocean color science and is used throughout these protocols.

<sup>3</sup> When the IOP are used in the context of a radiative transfer model, on the other hand, the translations and rotations relating local coordinates, used to describe scattering interactions (*e.g.* as at position  $\mathbf{x}_s^V$  in Fig. 1.3), to global coordinates, describing locations and directions in the medium as whole, become critically important.

<sup>4</sup> See Footnote 2 in (Vol. 1, Chapter 2) regarding the usage of the variable  $z$  in Fig. 2.2 and Sect. 2.4 of that chapter. Here we have substituted the symbol  $r$  for the optical pathlength along the  $z$ -axis in Fig. 1.3 (compare with Fig. 2.2 of Vol. 1 Ch. 2).

<sup>5</sup> The transmission of the illustrated beam of scattered photons to Detector 2 will be further considered as a starting point in the discussion of scattering measurement concepts in Sect. 1.5 below.

aforementioned “photon cloud” masking any indication of the vector nature of the scattered radiant field. Nevertheless, that mental construct is adequate for considering transmission measurement concepts. If the pathlength  $r_T$  is short enough that photons initially scattered out of the beam have a negligible chance of undergoing two (or more) additional scattering interactions that could return them to the beam, then it may be assumed that they will not be detected by Detector 1 (Fig. 1.4)<sup>6</sup>.

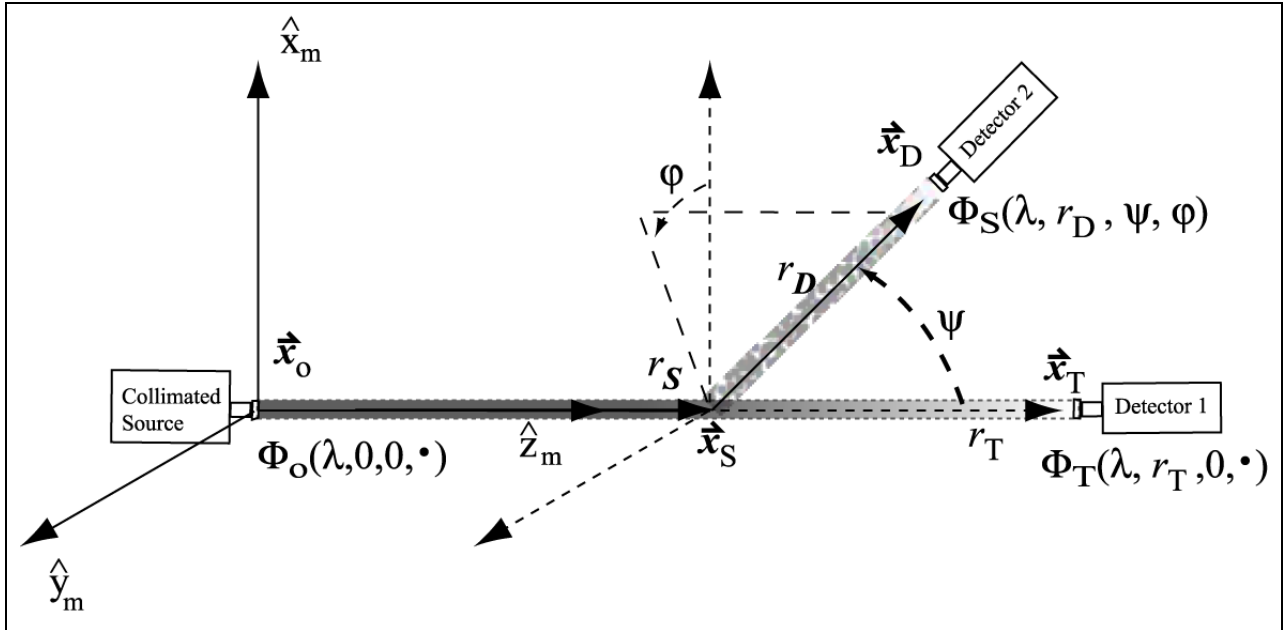


**Figure 1.4:** The local “Instrument Coordinate” framework describing optical beam transmission and scattering geometry. A collimated beam of radiometric flux  $\Phi_o(\lambda, 0, 0, \bullet)$  is emitted from a source at the origin  $\mathbf{x}_o$ . The flux within the collimated beam, shown schematically as a gradient shaded rectangle extending along the  $z_m$ -axis to Detector 1, is reduced by scattering and absorption as it is transmitted along the  $z_m$ -axis, and a reduced flux  $\Phi_T(\lambda, r_T, 0, \bullet)$  is measured by Detector 1 at position  $\mathbf{x}_T$ . At the intermediate location  $\mathbf{x}_S$ , some fraction of the flux  $\Phi_T(\lambda, r_S, 0, \bullet)$  that reaches that location is scattered out of the beam into direction  $(\psi, \phi)$ . The directionally scattered flux  $\Phi_S(\lambda, 0, \psi, \phi)$  is subsequently transmitted a distance  $r_D$  in that direction, with further losses due to scattering and absorption, and the reduced scattered flux  $\Phi_S(\lambda, r_D, \psi, \phi)$  is measured by Detector 2 at position  $\mathbf{x}_D$ . See text for further explanations.

The **beam attenuation coefficient** is defined in equations (2.16) through (2.18) of Vol. I, Chapter 2 (Sect. 2.4) as

$$c(\lambda) = a(\lambda) + b(\lambda), \text{ m}^{-1}, \quad (1.1)$$

where the **volume absorption** and **scattering coefficients**  $a(\lambda)$  and  $b(\lambda)$  are defined in terms of **absorptance**  $A(\lambda)$  and **scatterance**  $B(\lambda)$  in the limit of the optical pathlength  $\Delta r$  approaching zero as

$$a(\lambda) = \lim_{\Delta r \rightarrow 0} \frac{A(\lambda)}{\Delta r}, \text{ and } b(\lambda) = \lim_{\Delta r \rightarrow 0} \frac{B(\lambda)}{\Delta r}, \text{ m}^{-1}, \quad (1.2)$$

respectively. Equation (2.16) (Vol. I, Chapter 2) may be rearranged as

<sup>6</sup> The question, “What pathlength limit is ‘short enough’ to avoid multiply scattered photons from reaching a transmissometer’s detector?” is considered in Chapter 2 of this Protocol Volume.

$$\lim_{\Delta r \rightarrow 0} \left\{ \frac{\Phi_T(\lambda) - \Phi_i(\lambda)}{\Phi_i(\lambda) \Delta r} \right\} = \lim_{\Delta r \rightarrow 0} \left\{ -\frac{A(\lambda) + B(\lambda)}{\Delta r} \right\}, \quad (1.3)$$

where  $\Phi_i$  and  $\Phi_T$  are incident and transmitted radiant fluxes, respectively. Equation (1.3) may be expressed in differential form as

$$\frac{d\Phi(\lambda)}{\Phi(\lambda, r)} = -c(\lambda) dr. \quad (1.4)$$

Integrating (1.4) over an optical pathlength  $r_T$  as

$$c(\lambda) \int_0^{r_T} dr = -\int_0^{r_T} \frac{d\Phi(\lambda)}{\Phi(\lambda, r)}, \quad (1.5)$$

we obtain the solution for the beam attenuation coefficient

$$c(\lambda) = \frac{\ln \Phi_o(\lambda, 0, 0, \bullet) - \ln \Phi_T(\lambda, r_T, 0, \bullet)}{r_T} = \frac{-\ln T(\lambda, r_T)}{r_T} \text{ m}^{-1}, \quad (1.6)$$

where we adopt the conventions and notations described above and in Fig. 1.4. In (1.6), **transmittance**

$T(\lambda, r_T) \equiv \frac{\Phi_T(\lambda, r_T, 0, \bullet)}{\Phi_o(\lambda, 0, 0, \bullet)}$  is the fraction of radiant flux transmitted over the path distance  $r_T$ . Equation

(1.6) is the fundamental equation by which the **beam attenuation coefficient** is determined from a measurement made with a **transmissometer** (Chapter 2 of this volume).

The attenuation of radiant flux transmitted over a short optical pathlength  $r_T$  in seawater may be determined using the *Beer-Lambert-Bouguer Law* [equation (2.41), Vol. I, Ch. 2], which here follows directly from (1.6) as

$$\Phi_T(\lambda, r_T, 0, \bullet) = \Phi_o(\lambda, 0, 0, \bullet) e^{-c(\lambda)r_T}. \quad (1.7)$$

## 1.4 ABSORPTION MEASUREMENT CONCEPTS

### Reflecting Tube Absorption Meters

To determine the volume absorption coefficient  $a(\lambda)$  with a source and detector pair arranged on a common axis (*e.g.* the source and Detector 1 in Fig. 1.4), the flux reaching the detector window  $\Phi_K$  must include the sum of directly transmitted and scattered fluxes, *i.e.*  $\Phi_K = \Phi_T + \Phi_B$ . If the source and collector are equal in area and the water path between them (the shaded transmission path volume in Fig. 1.4) were enclosed in a perfectly reflecting tube, then all forward scattered photons would be redirected into the beam and reach the detector. For the present, we will postpone consideration of the flux loss due to backscattered photons and treat it as being negligible. Under this construct and assumption, equation (1.3) may be rewritten as

$$\lim_{\Delta r \rightarrow 0} \left\{ \frac{\Phi_T(\lambda) + \Phi_B(\lambda) - \Phi_i(\lambda)}{\Phi_i(\lambda) \Delta r} \right\} = -\lim_{\Delta r \rightarrow 0} \left\{ \frac{A(\lambda)}{\Delta r} \right\}, \quad (1.8)$$

expressed in differential form as

$$\frac{d\Phi_K(\lambda, r)}{\Phi(\lambda, r)} = -a(\lambda) dr, \quad (1.9)$$

and integrated over the path from 0 to  $r_T$  to obtain

$$a(\lambda) = \frac{\ln \Phi_o(\lambda, 0, 0, \bullet) - \ln \Phi_k(\lambda, r_T, 0, \bullet)}{r_T} = \frac{-\ln T_K(\lambda, r_T)}{r_T} \text{ m}^{-1}. \quad (1.10)$$

The reflecting tube method has been used to measure spectral absorption in the laboratory for many decades (James and Birge 1938). In recent years, this method has been adapted for use in the ocean (Zaneveld *et al.* 1992). Suitable instruments are now commercially available and are coming into general use within the oceanographic community. The best-known, commercially available example of this type of instrument is the “ac-9” manufactured by WET Labs Inc. of Philomath, OR. Protocols for calibrating and using reflecting tube absorption meters, and methods of data analysis are described in Chapter 3 of this volume, and in more specific detail for the ac-9 by Van Zee *et al.* (2002), which is available at ([www.wetlabs.com](http://www.wetlabs.com)).

### *Laboratory Methods for Determining Absorption Coefficients*

Protocols in Chapter 4, by Mitchell *et al.*, describe methods for filtering seawater to capture suspended particles on GF/F filters, and for measuring the absorption spectra of the particle-laden filters with a laboratory spectrophotometer. Methods are also described for extracting phytoplankton pigments from the filters, and measuring the residual absorption spectrum of particulate materials other than phytoplankton pigments. Finally, laboratory methods are also described for measuring the absorption spectrum of CDOM in filtered seawater samples. The material in this chapter derives from the results of recent experimental intercomparison workshops in which the authors participated, as well as from the published literature. Chapter 4 of this volume is a reformatted, but otherwise unchanged, version of Chapter 15 in Revision 3 to the ocean optics protocols (Mueller and Fargion 2002).

### *Absorption Determinations from Radiometric Measurements of Irradiance Flux Divergence*

*In situ* spectral absorption coefficient profiles can also be measured with spectral radiometers conforming to the performance specifications listed in Vol. II, Chapter 2, if the radiometric package is extended to measure  $E_d(z,\lambda)$  and  $E_u(z,\lambda)$ , as well as scalar irradiances  $\overset{\circ}{E}_d(z,\lambda)$  and  $\overset{\circ}{E}_u(z,\lambda)$ . This combination may be approached either using hemispherical collectors to measure upwelling and downwelling hemispherical irradiances (Hojerslev 1975), or by using cosine collectors on one radiometer in tandem with spherical collectors on another radiometer. Given these irradiance components, spectral absorption is then computed using Gershun's equation (Gershun 1939) as

$$a(z,\lambda) = \overset{\circ}{K}(z,\lambda) \frac{\overset{\circ}{E}(z,\lambda)}{\overset{\circ}{E}(z,\lambda)}, \quad (1.11)$$

where  $\overset{\circ}{E}(z,\lambda) = E_d(z,\lambda) - E_u(z,\lambda)$  is vector irradiance,  $\overset{\circ}{K}(z,\lambda)$  is the vertical attenuation coefficient for vector irradiance, and scalar irradiance  $\overset{\circ}{E}(z,\lambda) = \overset{\circ}{E}_d(z,\lambda) + \overset{\circ}{E}_u(z,\lambda)$  (see also Vol. I, Chapter 2).

Comparisons between absorption profiles measured using Gershun's equation with  $\overset{\circ}{E}(z,\lambda)$  and  $\overset{\circ}{E}(z,\lambda)$  (scalar irradiance) data, and absorption profiles measured with a reflecting tube instrument, agreed within 8% (Pegau *et al.* 1994). This level of agreement is well within the calibration uncertainties of the particular prototype instruments used for that experiment, which were approximately 10% uncertainties in both the scalar irradiance radiometer and in the reflecting tube instrument. Less than 5% uncertainties in absorption are expected in future experiments, assuming the data are properly averaged to remove near-surface irradiance fluctuations caused by surface waves (Zaneveld *et al.* 2001). In very clear oligotrophic water, moreover, uncertainty in water absorption values may make it impossible to realize this level of relative agreement.

### *Other Methods of Measuring Absorption*

There are several other measurement concepts that may be used to determine the absorption coefficient of seawater, however, none of them are currently useful for making routine measurements during daylight conditions at sea. One possible exception is the determination of absorption by inverting radiance distribution profiles measured using a camera system (Voss 1989), but at present, such camera systems are not commercially available<sup>7</sup>. In a similar method, absorption may be determined by inverting the radiative transfer equation for several measured moments of an axially symmetric radiance distribution in the asymptotic regime (Zaneveld and Pak 1972; Wells 1983). Other examples include the determination  $a_w(\lambda)$  using an integrating cavity (Pope and Fry 1997), photothermal methods (Sogandares and Fry 1997), and differential optoacoustic spectroscopy (Voss and Trees 1987). Optoacoustic spectroscopy was also

---

<sup>7</sup> It would be advantageous were this situation to change in the future, as such camera systems are potentially even more useful for determining the Bidirectional Reflectance Distribution Function (BRDF) and Exact Normalized Water-Leaving Radiance (Vol. III, Ch. 4).

used to measure  $a_p(\lambda)$  in phytoplankton cultures (Trees and Voss 1990). Absorption may also be determined from measurements of irradiance divergence from a submerged isotropic source (Maffione *et al.* 1993, and earlier references cited there). The present version of this volume does not address any of these methods.

## 1.5 SCATTERING MEASUREMENT CONCEPTS

### *Scattering Coefficient Determinations*

There is no practical way to directly measure the volume scattering coefficient  $b(\lambda)$ . Given measurements of absorption and beam attenuation coefficients, however, the volume scattering coefficient may be computed from (1.1) as  $b(\lambda) = c(\lambda) - a(\lambda)$ ,  $m^{-1}$ . In practice it's not quite that simple, and several interrelated scattering and absorption corrections must be applied (Chapters 3 and 5 in this Volume). Alternatively, attempts have been made to calculate  $b(\lambda)$  by integrating measurements of the VSF, *e.g.*, by Petzold (1972).

### *Volume Scattering Function Measurements*

In Fig. 1.4, the combination of the source at  $\mathbf{x}_o$ , directional scattering at  $\mathbf{x}_s$ , and Detector 2 at location  $\mathbf{x}_D$  schematically illustrate the conceptual elements of a scattering meter designed to measure the VSF  $\beta(\lambda, \psi, \varphi)$ . Collimated flux  $\Phi_o(\lambda, 0, 0, \bullet)$  is transmitted, in a beam of cross-sectional area  $A$ , from the source to  $\mathbf{x}_s$  as

$$\Phi_T(\lambda, r_s, 0, \bullet) = \Phi_o(\lambda, 0, 0, \bullet) e^{-c(\lambda)r_s}. \quad (1.12)$$

The irradiance incident normal to the optical transmission axis at  $\mathbf{x}_s$  is

$$E_i = \frac{\Phi_T(\lambda, r_s, 0, \bullet)}{A} = \frac{\Phi_o(\lambda, 0, 0, \bullet) e^{-c(\lambda)r_s}}{A}. \quad (1.13)$$

At position  $\mathbf{x}_s$ , some of the incident radiant flux is scattered in direction  $(\psi, \varphi)$ , into the solid angle field-of-view  $\Omega_{FOV}$  of Detector 1, from the volume  $V(\psi)$  defined by the intersection of the beam and detector field of view. The radiant intensity of the scattered flux is

$$I_s(\lambda, \psi, \varphi) = \frac{\Phi_s(\lambda, 0, \psi, \varphi)}{\Omega_{FOV}}, \quad (1.14)$$

and scattered flux reaching the detector is

$$\Phi_s(\lambda, r_D, \psi, \varphi) = \Phi_s(\lambda, 0, \psi, \varphi) e^{-c(\lambda)r_D}. \quad (1.15)$$

From equation (2.30) we may determine the VSF averaged over the working volume and solid angle FOV approximately as

$$\bar{\beta}(\lambda, \psi, \varphi) \cong \frac{I_s(\lambda, 0, \psi, \varphi)}{E_i V(\psi)}, \quad (1.16)$$

or by substituting from (1.12) through (1.13), directly in terms of source and detector fluxes as

$$\bar{\beta}(\lambda, \psi, \varphi) \cong \frac{\Phi_s(\lambda, r_D, \psi, \varphi) A}{\Phi_o(\lambda, 0, 0, \bullet) V(\psi) \Omega_{FOV}} e^{-c(\lambda)(r_s - r_D)}. \quad (1.17)$$

One must know both  $c(\lambda)$  and  $\Phi_o(\lambda, 0, 0, \bullet)$  to determine the VSF from (1.17). If the same detector were used at positions shown for detectors 1 and 2 in Fig. 1.4, following the method introduced by Kullenberg (1968), and if  $r_D = r_T - r_s$ , we may substitute from (1.7) and determine the VSF from the two measured detector fluxes as

$$\bar{\beta}(\lambda, \psi, \varphi) \equiv \frac{\Phi_s(\lambda, r_D, \psi, \varphi) A}{\Phi_T(\lambda, r_T, 0, \bullet) V(\psi) \Omega_{\text{FOV}}}. \quad (1.18)$$

Equation (1.18) could be used to measure the VSF if the source and detector are well collimated, and there were no flux losses, or FOV distortions, associated with an instrument's optical assembly. For most scattering meters, however, the averaged VSF estimate  $\bar{\beta}(\lambda, \psi, \varphi)$  is related to the true VSF  $\beta(\lambda, \psi, \varphi)$  by a weighted integral

$$\bar{\beta}(\lambda, \psi, \varphi) = \int_0^{2\pi} \int_0^{\pi} \beta(\lambda, \psi, \varphi) W(\lambda, \psi, \varphi; c) \sin \psi d\psi d\varphi. \quad (1.19)$$

where the weighting function  $W(\lambda, \psi, \varphi; c)$  accounts for instrumental factors including the divergence and uniformity of the source beam and detector angular response function, the working volume geometry, variations in attenuation of flux scattered to the detector from different volume elements, and optical reflection and absorption losses in the system. Practical methods for determining  $W(\lambda, \psi, \varphi; c)$  are described in Chapter 5.

The VSF of ocean water is usually considered to be azimuthally symmetric about the transmission axis. Therefore, the VSF is usually reported as  $\beta(\lambda, \psi)$ , which is a function of the polar "scattering angle" alone. In terms of the VSF measurements as represented in (1.19), we have that

$$\bar{\beta}(\lambda, \psi) = \int_0^{2\pi} \bar{\beta}(\lambda, \psi, \varphi) d\varphi = 2\pi \bar{\beta}(\lambda, \psi, \varphi). \quad (1.20)$$

### *Backscattering Coefficient Determination*

The backscattering coefficient  $b_b(\lambda)$  [Vol. I, Ch. 2, equation (2.23)] is an important factor in the physical relationship between the IOP and remote sensing reflectance (Vol. III, Ch. 4, Sect. 4.3 and references cited therein). As is the case for the volume scattering coefficient  $b(\lambda)$ , there is no practical way to directly measure  $b_b(\lambda)$  in the sea. If that is true, then how can  $b_b(\lambda)$  be determined using the so-called "backscattering meters" in common use within the community? These instruments actually measure the VSF  $\bar{\beta}(\lambda, \psi)$  at one angle  $\psi^*$ , or several angles  $\psi_i^*, i=1, 2, K, N$ , in the backward direction. For single angle VSF instruments, such as the HOBILABS HydroScat-series and WET Labs ECO-BB series, one uses the fact that most observed phase functions and modeled VSFs show a common crossover angle  $\psi^*$  at which  $\bar{\beta}(\lambda, \psi^*) \propto b_b(\lambda)$ . An empirical linear equation is used to calculate  $b_b(\lambda)$  from  $\bar{\beta}(\lambda, \psi^*)$ ; where the angle  $\psi^*$  is selected to minimize the uncertainty in  $b_b(\lambda)$  associated with a simulated uncertainty in  $\beta_p^{\circ}(\lambda, \psi)$  (Oishi 1990; Maffione and Dana; Boss and Pegau 2001). The approach used to determine  $b_b(\lambda)$  from measurements of  $\bar{\beta}(\lambda, \psi_i, \varphi); i=1, 2, K, N$  angles, *e.g.* using a WET Labs VSF-3, is to fit a polynomial to the  $N+1$  values  $2\pi \bar{\beta}(\lambda, \psi_i, \varphi) \sin \psi_i$  derived from the  $N$  measurements and the endpoint  $2\pi \bar{\beta}(\lambda, \pi, \bullet) \sin \pi \equiv 0$  and integrate it from  $\frac{\pi}{2}$  to  $\pi$  (following Beardsley and Zaneveld 1969).

## REFERENCES

- Beardsley, G.F. and J.R.V. Zaneveld, 1969: Theoretical dependence of the near-asymptotic apparent optical properties of sea water. *J. Opt. Soc. Amer.* 59: 373-377.
- Boss, E. and W.S. Pegau, 2001: Relationship of light scattering at an angle in the backward direction to the backscattering coefficient. *Appl. Opt.*, **40**: 5503-5507.
- Bogucki, D.J., J.A. Domaradzki, D. Stramski and J.R.V. Zaneveld, 1998. Comparison of near-forward light scattering on oceanic turbulence and particles. *Appl. Opt.*, **37(21)**: 4669-4677.

- Bricaud, A., A. Morel and L. Prieur, 1981. Absorption by dissolved organic matter of the sea (yellow substance) in the UV and visible domains. *Limnol Oceanogr*, **26(1)**: 43-53.
- Buiteveld, H., J.H.M. Hakvoort and M. Donze, 1994: The optical properties of pure water. *Ocean Optics XII*, SPIE Vol. 2258: 174-183.
- Gordon, H.R. and A. Morel, 1983: *Remote Assessment of Ocean Color for Interpretation of Satellite Visible Imagery, a Review; Lecture Notes on Coastal and Estuarine Studies, Vol. 4*, Springer Verlag, New York, 114pp.
- Gershun, A., 1939: The light field. *J. Math. Phys.* **18**: 51-151.
- Hojerslev, N.K., 1975: A spectral light absorption meter for measurements in the sea. *Limnol. Oceanogr.*, **20**: 1024-1034.
- James, H.R., and E.A. Birge, 1938: A laboratory study of the absorption of light by lake waters. *Trans. Wis. Acad. Sci.*, **31**: 1--154.
- Kou, L., D. Labrie and P. Chylek, 1993: Refractive indices of water and ice in the 0.65 to 2.5  $\mu\text{m}$  spectral range, *Appl. Opt.*, **32**: 3531-3540.
- Kullenberg, G., 1968: Scattering of light by Sargasso Sea water, *Deep-Sea Res.*, **15**: 423-432.
- Maffione, R.A. and D.R. Dana, 1997: Instruments and methods for measuring the backward-scattering coefficient of ocean waters. *Appl. Opt.* **36**: 6057-6067.
- Maffione, R.A., K.J. Voss and R.C. Honey, 1993. Measurement of the spectral absorption coefficient in the ocean with an isotropic source. *Appl. Opt.*, **32(18)**: 3273-3279.
- Morel, A., 1974: Optical properties of pure water and pure sea water. In: *Optical Aspects of Oceanography*, N.G. Jerlov and E.S. Nielson, Eds., pp1-23.
- Morel, A. and S. Maritorena, 2001. Bio-optical properties of oceanic waters: A reappraisal, *J. Geophys. Res.*, **106(C4)**: 7163-7180.
- Mueller, J.L. and G.S. Fargion,[Eds.], 2002: Ocean Optics Protocols for Satellite Ocean Color Sensor Validation, Revision 3. *NASA Tech. Memo. 2002-210004*, NASA Goddard Space Flight Center, Greenbelt, Maryland, 308pp.
- Oishi, T., 1990. Significant relation between the backward scattering coefficient of sea water and the scatterance at 120 degrees. *Appl. Opt.*, **29(31)**: 4658-4665.
- Pegau, W.S. and J.R.V. Zaneveld, 1993: Temperature dependent absorption of water in the red and near infrared portions of the spectrum. *Limnol. Oceanogr.*, **38(1)**: 188-192.
- Pegau, W.S., J.S. Cleveland, W. Doss, C.D. Kennedy, R.A. Maffione, J.L. Mueller, R. Stone, C.C. Trees, A.D. Weidemann, W.H. Wells, and J.R.V. Zaneveld, 1995: A comparison of methods for the measurement of the absorption coefficient in natural waters. *J. Geophys. Res.*, **100(C7)**: 13,201-13,220.
- Pegau, W.S., D. Gray and J.R.V. Zaneveld, 1997: Absorption and attenuation of visible and near-infrared light in water: dependence on temperature and salinity. *Appl. Opt.*, **36(24)**: 6035-6046.
- Petzold, T.J., 1972. Volume scattering functions for selected ocean waters. Contract No. N62269-71-C-0676, UCSD, SIO Ref. 72-78.
- Pope, R.M. and E.S. Fry. 1997: Absorption spectrum (380-700 nm) of pure water. II. Integrating cavity measurements. *Appl. Opt.* **36**: 8710-8723.
- Prieur, L. and S. Sathyendranath, 1981. An optical classification of coastal and oceanic waters based on the specific spectral absorption curves of phytoplankton pigments, dissolved organic matter, and other particulate materials. *Limnol. Oceanogr.*, **26(4)**: 671-689.
- Smith, R.C. and K.S. Baker, 1981. Optical properties of the clearest natural waters (200-800 nm), *Appl Opt.* **20 (2)**: 177-184.

- Sogandares, F.M. and E.S. Fry, 1997. Absorption spectrum (340-640 nm) of pure water. I. Photothermal measurements. *Appl. Opt.*, **36(33)**: 8699-8709.
- Trees, C.C. and K.J. Voss, 1990. Optoacoustic spectroscopy and its application to molecular and particle absorption. *OCEAN OPTICS X*, SPIE **1302**: 149-156.
- Voss, K.J., 1989: Use of the radiance distribution to measure the optical absorption coefficient in the ocean, *Limnol. Oceanogr.*, **34**: 1614-1622.
- Van Zee, H., D. Hankins, and C. deLespinasse, 2002: *ac-9 Protocol Document (Revision F)*. WET Labs Inc., Philomath, OR, 41pp.
- Wells, W.H., 1983: Techniques for measuring radiance in sea and air. *Appl. Opt.*, **22**: 2313-2321.
- Zaneveld, J.R.V., E. Boss and A. Barnard, 2001. Influence of surface waves on measured and modeled irradiance profiles. *Appl. Opt.*, **40(9)**: 1442-1449.
- Zaneveld, J.R.V., J.C. Kitchen, A. Bricaud, and C. Moore, 1992: Analysis of *in situ* spectral absorption meter data. *Ocean Optics XI*, G.D. Gilbert, Ed., SPIE, 1750, 187--200.
- Zaneveld, J.R.V., and H. Pak, 1972. Some aspects of the axially symmetric submarine daylight field. *J. Geophys. Res.*, **77(15)**: 2677-2680.